Identification and characterization of hydrophobic gate residues in TRP channels

Wang Zheng,[*,†] Ruikun Hu,[‡] Ruiqi Cai,[†] Laura Hofmann,[§] Qiaolin Hu,[†] Mohammad Fatehi,[¶] Wentong Long,[¶] Tim Kong,[†] Jingfeng Tang,[*,1] Peter Light,[¶] Veit Flockerzi,[§] Ying Cao,[‡] and Xing-Zhen Chen[†,2]

[*]Institute of Biomedical and Pharmaceutical Sciences, Key Laboratory of Fermentation Engineering of Ministry of Education, College of Bioengineering, Hubei University of Technology, Wuhan, China; [†]Membrane Protein Disease Research Group, Department of Physiology, and [¶]Department of Pharmacology, Faculty of Medicine and Dentistry, University of Alberta, Edmonton, Alberta, Canada; [‡]School of Life Sciences and Technology, Tongji University, Shanghai, China; and [§]Experimentelle und Klinische Pharmakologie und Toxikologie, Universität des Saarlandes, Homburg, Germany

ABSTRACT: Transient receptor potential (TRP) channels, subdivided into 6 subfamilies in mammals, have essential roles in sensory physiology. They respond to remarkably diverse stimuli, comprising thermal, chemical, and mechanical modalities, through opening or closing of channel gates. In this study, we systematically substituted the hydrophobic residues within the distal fragment of pore-lining helix S6 with hydrophilic residues and, based on *Xenopus* oocyte and mammalian cell electrophysiology and a hydrophobic gate theory, identified hydrophobic gates in TRPV6/V5/V4/C4/M8. We found that channel activity drastically increased when TRPV6$_{Ala616\ or\ Met617}$ or TRPV5$_{Ala576\ or\ Met577}$, but not any of their adjacent residues, was substituted with hydrophilic residues. Channel activity strongly correlated with the hydrophilicity of the residues at those sites, suggesting that consecutive hydrophobic residues TRPV6$_{Ala616\text{-}Met617}$ and TRPV5$_{Ala576\text{-}Met577}$ form a double-residue gate in each channel. By the same strategy, we identified a hydrophobic single-residue gate in TRPV4$_{Iso715}$, TRPC4$_{Iso617}$, and TRPM8$_{Val976}$. In support of the hydrophobic gate theory, hydrophilic substitution at the gate site, which removes the hydrophobic gate seal, substantially increased the activity of TRP channels in low-activity states but had little effect on the function of activated channels. The double-residue gate channels were more sensitive to small changes in the gate's hydrophobicity or size than single-residue gate channels. The unconventional double-reside gating mechanism in TRP channels may have been evolved to respond especially to physiologic stimuli that trigger relatively small gate conformational changes.—Zheng, W., Hu, R., Cai, R., Hofmann, L., Hu, Q., Fatehi, M., Long, W., Kong, T., Tang, J., Light, P., Flockerzi, V., Cao, Y., Chen, X.-Z. Identification and characterization of hydrophobic gate residues in TRP channels. FASEB J. 32, 639–653 (2018). www.fasebj.org

KEY WORDS: electrophysiology · *Xenopus* oocyte · hydrophobicity · hydrophilicity

With few exceptions, mammalian transient receptor potential (TRP) channels are a superfamily of nonselective cation channels found in almost all cell types (1). They are divided into 6 subfamilies, named after the first described member of each subfamily: vanilloid (TRPV), polycystin (TRPP), canonical (TRPC), melastatin (TRPM), ankyrin (TRPA), and mucolipin (TRPML). TRP channels are tetramers in which each subunit has 6 transmembrane segments (S1–S6) and cytosolic amino- and carboxy-termini (2). S5, S6, and the S5–S6 pore loop of each subunit form the central pore module, surrounded by S1–S4 (2). Although sharing similar structural arrangements with voltage-gated cation channels, TRP channels respond to remarkably diverse stimuli, which include pH, temperature, touch, osmolarity, pheromones, and noxious chemicals (3–7). Numerous studies have established that TRP channels fulfill salient roles in sensory physiology, such as sensations of pain, hotness, warmth and coldness, tastes, pressure, and vision (3–6). Mutations in TRP genes have been linked to an inherited pain syndrome, skeletal dysplasia, kidney disorders, and, likely, cancer (8–10). Although TRP channels have recently been among the most intensively pursued drug targets (11), our understanding of their gating mechanisms and of the way in which they respond to such diverse types of stimulatory inputs lags far behind and requires a systematic correlation of their structure and function.

ABBREVIATIONS: DVF, divalent-free; GSK, GSK1016790A; HEK, human embryonic kidney; HEPES, 4-(2-hydroxyethyl)piperazine-1-ethanesulfonic acid; kHz, kilohertz; SCAM, substituted-cysteine accessibility method; TRP, transient receptor potential; TRPA, TRP ankyrin; TRPC, TRP canonical; TRPM, TRP melastatin; TRPML, TRP mucolipin; TRPP, TRP polycystin; TRPV, TRP vanilloid; WT, wild type

[1] Correspondence: Hubei University of Technology, Wuhan, China. E-mail: jingfeng9930@163.com

[2] Correspondence: University of Alberta, 7-29A Medical Sciences, Edmonton, AB T6G 2H7, Canada. E-mail: xzchen@ualberta.ca

doi: 10.1096/fj.201700599RR

This article includes supplemental data. Please visit *http://www.fasebj.org* to obtain this information.

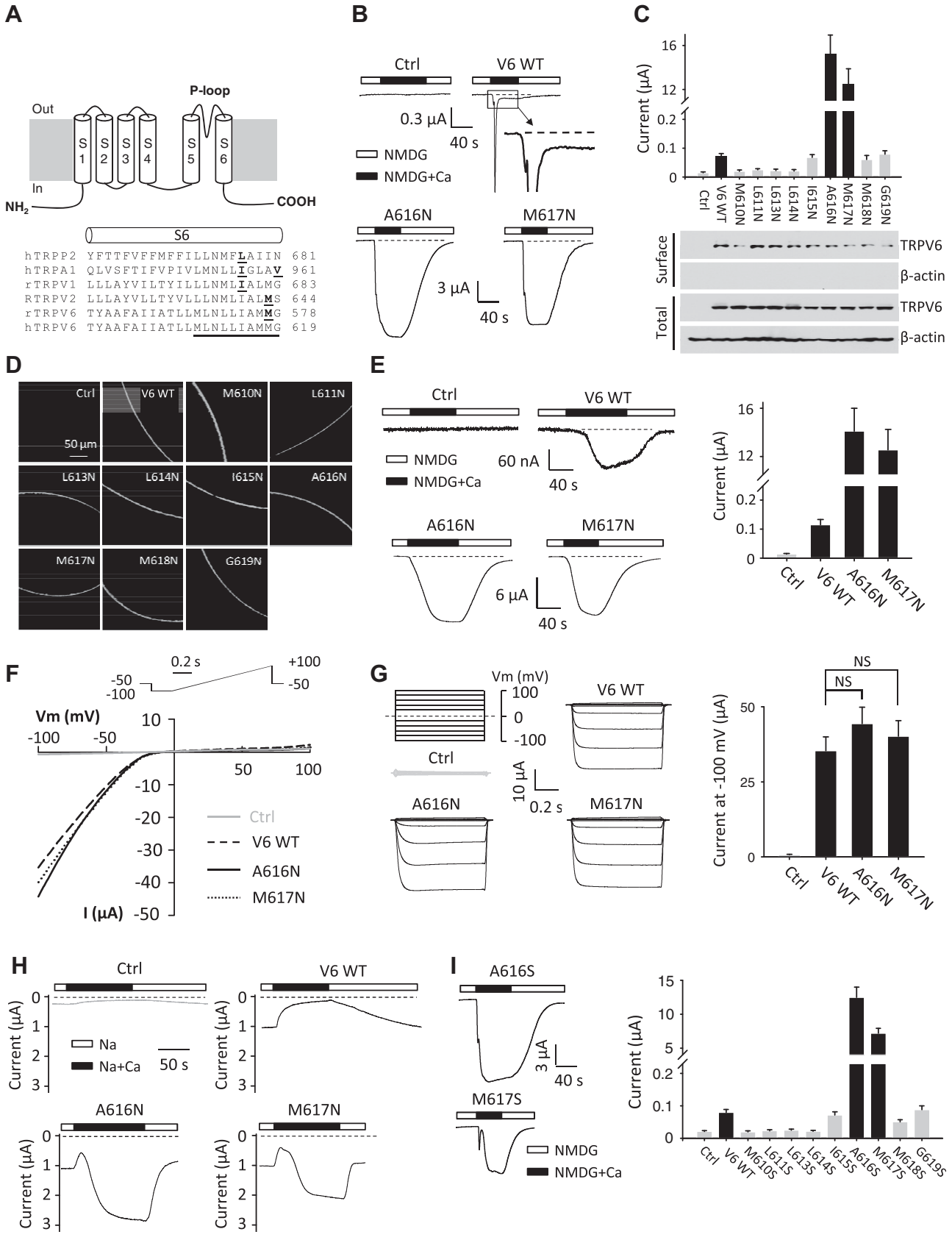

Figure 1. Functional characterization of human TRPV6 channels carrying point mutations at, and adjacent to, the putative lower-gate region. *A*) Membrane topology of a single TRP protein and amino acid sequence alignment of the S6 helix of the 5 TRP channels with structures that were recently solved [hTRPV2 (12), hTRPA1 (16), rTRPV1 (15), RTRPP2 (17), rTRPV6 (13); r, rat; h, human; R, rabbit]. The residues that are assumed to form the lower gate are marked in bold and underlined. Each single

(*continued on next page*)

Ion channels control ion flow by opening or closing an activation gate, the region preventing ions passing through the channel's pore in the closed state. Structural determination of TRPV1, TRPV2, TRPV6, TRPA1, and TRPP2 revealed that the ion permeation pore in TRP channels, like that of voltage-gated cation channels, is characterized by the presence of a selectivity filter, sometimes called an upper gate, formed by the 4 intervening S5–S6 loops and a constriction, called a pore gate or lower gate, formed by the cytoplasmic end of each of the 4 pore-lining S6 helices (12–19). Voltage-gated sodium and calcium channels have been shown to possess an evolutionarily conserved, hydrophobic lower gate in the pore-lining transmembrane helix (20, 21). In voltage-gated potassium channels, a highly conserved Pro-Val-Pro (PVP) motif in S6 is thought to form a tight, hydrophobic seal (21, 22) because changing those residues to hydrophilic residues opens the channel at resting voltages (23, 24). In comparison, the nature and the location of gates in TRP channels have remained more elusive.

Based on the hydrophobic gate theory (25), a hydrophobic gate closes the pore through the so-called liquid–vapor transition of water molecules within the gate region, rather than through physical, steric occlusion of the pore. These transient vapor states are devoid of water molecules within the hydrophobic gate region, which causes an energetic barrier to ion conduction. Molecular dynamics simulations showed that the hydration rate is close to zero when the gate region has a physical diameter of <9 Å (closed state) and dramatically increases to the maximum when it reaches 12–13 Å (open state) in a strong, sigmoidal dependence (25). In this dynamic range of the gate region (9–13 Å), the ion conduction ($\propto$ hydration rate $\times$ pore size) could increase substantially without a drastic gain in pore size, which explains well the observed pore sizes of the crystallized, bacterial, small-conductance, mechanosensitive channel MscS in closed (8 Å) and open (13 Å) states (26, 27). In fact, the open-state pore sizes of several TRP channels were all found to be within the 11–13 Å range (28–31). In contrast, simulation studies also showed that replacement of the hydrophobic gate with a hydrophilic residue drastically increased the pore hydration rate and, consequently, ion flow (25). Thus, channels can be opened by increasing either the pore diameter defined by the gate (*i.e.*, *via* conformational changes induced by stimuli) or the hydrophilicity of the gate residue (*i.e.*, *via* mutations) (25). The latter procedure has led to identification of a hydrophobic barrier deep within the inner pore of the TWIK-1 K2P potassium channel responsible for its low levels of functional activity (32).

The distal amino acid sequence of the pore-lining helix S6 is one of the few sequences shared by TRP channels and contains a conserved pattern (which we call a gate motif) containing 6 consecutive hydrophobic residues bracketed by 2 hydrophilic residues (Supplemental Fig. S1). The recently resolved structures of several TRP channels revealed gate residues that are all within the motif (12, 13, 15–17), but they did not always find the same or corresponding gate residues that sequence homology would predict (**Fig. 1*A***). In this study, we systematically substituted residues in the distal part of the S6 helix (within or around the gate motif) in 5 members from 3 TRP subfamilies—TRPV6, TRPV5, TRPV4, TRPC4, and TRPM8—with hydrophilic residues and studied the effects on channel activity, using the 2-electrode voltage clamp in *Xenopus laevis* oocytes, a patch clamp in human embryonic kidney 293 (HEK293) cells, biotinylation, and immunofluorescence, to identify and characterize the lower gate residues. We reasoned that changing the gate residue in TRP channels, but not the adjacent residues, would give rise to constitutive opening of channels in low-activity states when its hydrophilicity is increased. We discuss our data in view of available TRP structures and the substituted-cysteine accessibility method (SCAM) studies, compare characteristic

underlined amino acid of human TRPV6 (hTRPV6) was mutated to asparagine (N). *B*) Representative membrane currents recorded in voltage-clamped oocytes at −50 mV injected with cRNA of hTRPV6 WT or mutants A616N or M617N. Water-injected oocytes were used as control (ctrl). The extracellular solution contained (mM): 100 *N*-methyl-D-glucamine (NMDG)-Cl, 2 KCl, 1 $MgCl_2$, 10 HEPES (pH 7.5) (NMDG), or the NMDG solution, including 5 mM $CaCl_2$ (NMDG + Ca). Dashed lines are the baselines from which the plateau current values were determined. Bottom: representative Western blot of surface biotinylated (surface) and total TRPV6 proteins (total), as indicated. β-actin was used as a control. *C*) Averaged plateau current amplitudes obtained from oocytes injected with the cRNA of WT or mutant channels, or from water-injected oocytes (ctrl), similar to that in panel *B* (means ± SEM; $n = 15$–21). Oocytes were from ≥3 batches. *D*) Representative whole-mount immunofluorescence using the anti-TRPV6 antibody showing the oocyte surface expression of the mutants from panel *C*. *E*) Left: representative current traces recorded at −50 mV from water-injected oocytes (ctrl) or oocytes injected with cRNA of hTRPV6 WT or mutant A616N or M617N. Oocytes were preinjected with 25 nl of 50 mM EGTA ≥2 h before current measurements. Right: averaged plateau current amplitudes obtained under the same experimental conditions as in the left panel ($n = 10$–12). *F*) Representative *I–V* curves obtained from water-injected oocytes (ctrl) or those expressing hTRPV6 WT or mutant A616N or M617N using a ramp protocol, as indicated, in the presence of DVF extracellular solution containing the following (mM): 100 NaCl, 2 KCl, 1 ETGA, 10 HEPES (pH 7.5). *G*) Left: representative membrane currents obtained using a jump protocol, as indicated, in the presence of the DVF extracellular solution. Right: averaged plateau current amplitudes at −100 mV obtained under the same experimental conditions as in the left panel ($n = 9$–14). NS, not significant. *H*) Representative current traces at −30 mV obtained from water-injected oocytes (ctrl) or oocytes injected with cRNA of hTRPV6 WT or mutant A616N or M617N. Oocytes were preinjected with 25 nl of 50 mM EGTA ≥2 h before current measurements, in the presence of the Na^+-containing solution (Na) with the following (mM): 100 NaCl, 2 KCl, 10 HEPES (pH 7.5), with (Na + Ca) or without (Na) 5 mM $CaCl_2$. *I*) Left: representative membrane currents measured at −50 mV in oocytes expressing hTRPV6 mutant A616S or M617S. Right: similar to panel *C*, averaged currents for the indicated single mutants ($n = 14$–21).

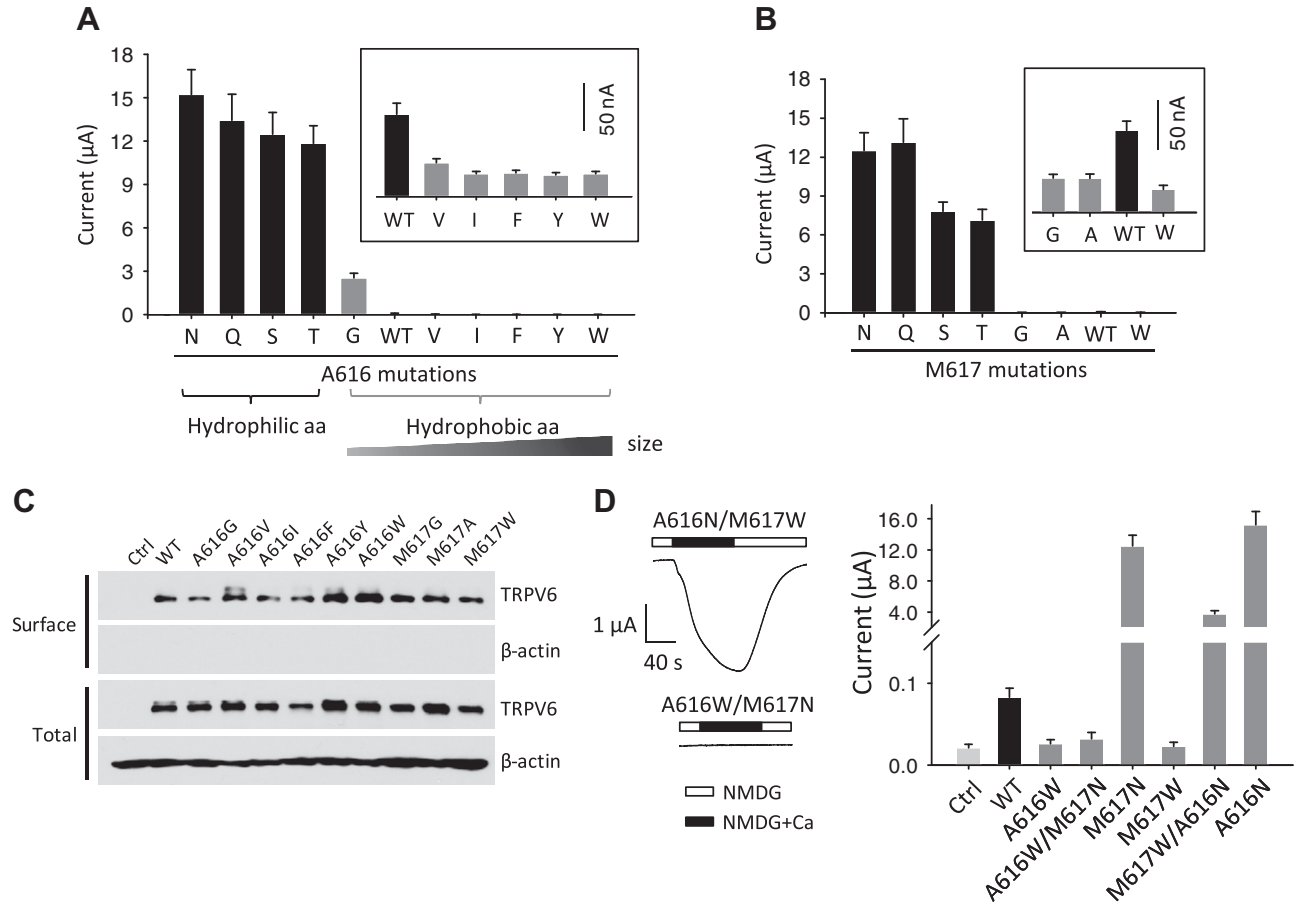

Figure 2. Characterization of point mutants at gate sites A616 and M617 of human TRPV6. *A*) A616 was replaced by the indicated amino acid (aa) and the averaged currents obtained, as shown in Fig. 1*C* (n = 17–20 oocytes from ≥3 batches). *B*) M617 was replaced by different amino acid, as indicated; the resulting membrane currents from different mutants were recorded and averaged as in Fig. 1*C* (n = 15–20). Bar graph with a different current scale (inset). *C*) Western blot of surface-biotinylated and total TRPV6 WT or mutants, as indicated. Bar graph with a different current scale (inset). *D*) Left: representative current traces obtained at −50 mV as in Fig. 1*B* in oocytes injected with the TRPV6 double-mutant A616N/M617W or A616W/M617N. Right: averaged currents of the indicated mutants as in Fig. 1*C*.

differences between single- and double-residue gates, and compare the distinct effects of hydrophilic gate mutations when channels are in resting or activated states.

MATERIALS AND METHODS

Plasmids, mutants, antibodies, and chemicals

Human TRPV6 (accession: NM_018646; GenBank, National Center for Biotechnology Information, Bethesda, MD, USA; *http://www.ncbi.nlm.gov/genbank/*) and mouse TRPC4 (NM_001253682) cDNAs were subcloned into oocyte expression vectors pBSMXT-MCS and pSGEM, respectively. The mouse TRPC4 cDNA was subcloned into the mammalian expression vector pMax-IRES-GFP for expression in HEK293 cells. Rat TRPM8 (NM_134371) plasmid was kindly provided by Dr. David Julius (University of California, San Francisco, San Francisco, CA, USA). Human TRPV5 (NM_019841) and Rat TRPV4 (NM_023970) plasmids were from Dr. Ji-Bin Peng (University of Alabama, Birmingham, Birmingham, AL, USA) and Dr. Ching Kung (University of Wisconsin-Madison, Madison, WI, USA), respectively. All mutations were made with QuikChange Lightning Site-Directed Mutagenesis Kit (Agilent Technologies, Santa Clara, CA, USA) and confirmed by sequencing. Mouse antibody against β-actin (C-4) was purchased from Santa Cruz Biotechnology (Santa Cruz, CA, USA). Rabbit antibodies against TRPC4 (ab83689) and TRPM8 (ab3243) were purchased from Abcam Inc (Milton, Cambridge, United Kingdom). Antibodies against TRPV6 and TRPC4 were generated in house (33, 34). Rabbit anti-TRPV5 antibody (CAT21-S) was purchased from Alpha Diagnostic International (San Antonio, TX, USA). Secondary antibodies were purchased from GE Healthcare Life Sciences (Little Chalfont, United Kingdom). GSK1016790A (GSK), a TRPV4 agonist, and menthol, a TRPM8 agonist, were purchased from Sigma-Aldrich (St. Louis, MO, USA).

Xenopus oocyte expression

Capped synthetic RNA of TRPV6, TRPV5, TRPV4, TRPC4, and TRPM8 were synthesized by *in vitro* transcription with mMessage mMachine Kit (Ambion, Austin, TX, USA) and injected (25–50 ng/oocyte) into *Xenopus laevis* oocytes prepared as described in Zheng *et al.* (35). Equal volumes of water were injected into control oocytes. Experiments were performed 1–3 d after injection. The present study was approved by the Ethical Committee for Animal Experiments of the University of Alberta, and was performed in accordance with the Guidelines for Research with Experimental Animals of the University of Alberta

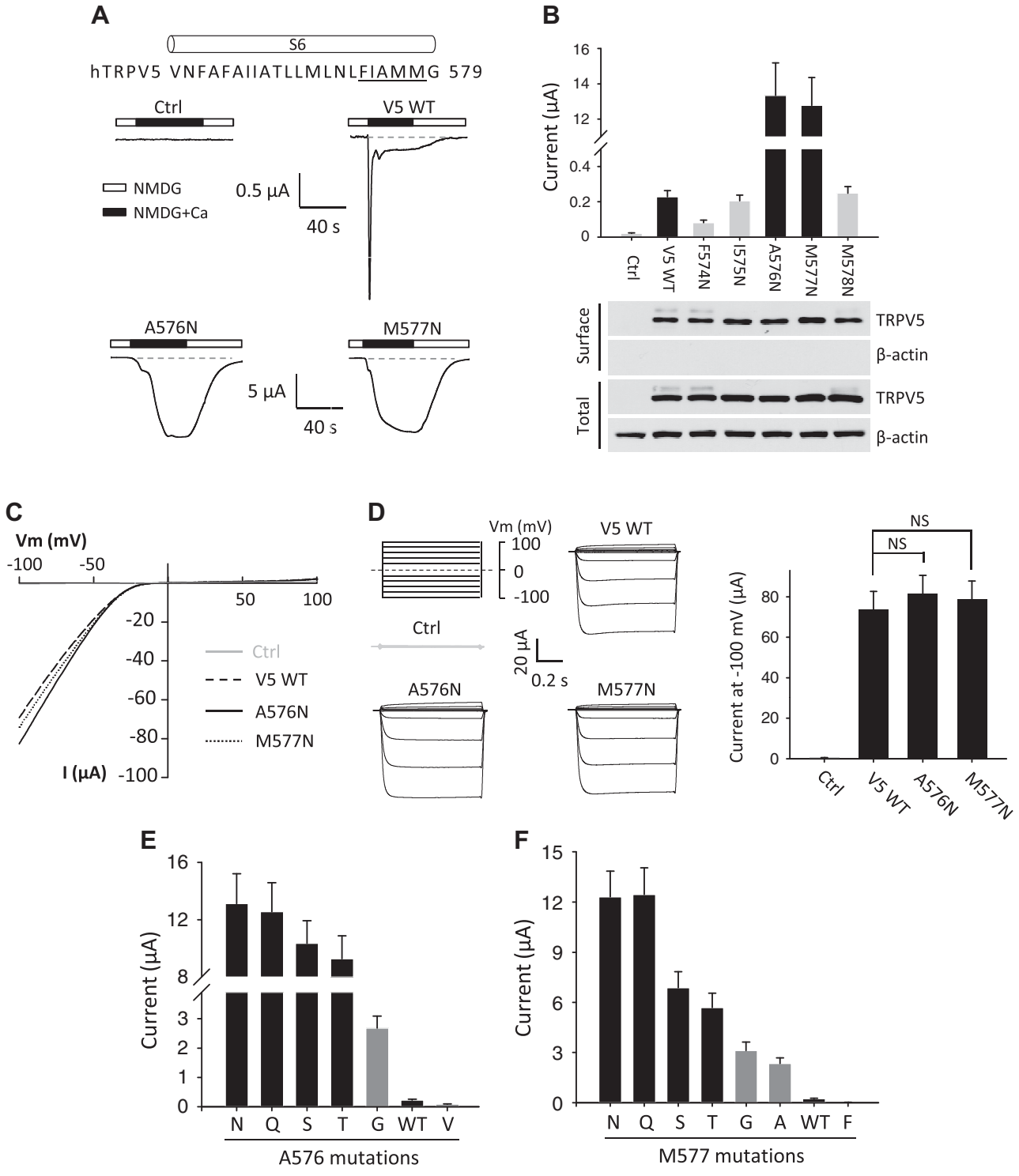

Figure 3. Characterization of point mutants at, and adjacent to, the putative gate region in S6 of human TRPV5. *A*) Each single underlined amino acid of TRPV5 was mutated to N. Representative membrane currents recorded in voltage-clamped oocytes at −50 mV injected with cRNA of human TRPV5 WT or mutants A576N or M577N. Water-injected oocytes were used as control (ctrl). The extracellular NMDG and NMDG + Ca solutions are the same with those in Fig. 1*B*. Dashed lines are the baselines from which plateau current values were determined. *B*) Top: averaged plateau current amplitudes obtained from oocytes injected with the cRNA of TRPV5 WT or mutant channels, or from water-injected oocytes (ctrl) (means ± SEM; n = 13–20). Oocytes were from ≥3 batches. Bottom: representative Western blot of surface-biotinylated and total TRPV5 proteins, as indicated. β-actin was used as a control. *C*) Representative *I–V* curves obtained from oocytes expressing hTRPV5 WT, mutant A576N or mutant M577N, or water-injected oocytes (ctrl), in the presence of the DVF extracellular solution. *D*) Left: representative membrane currents obtained from water-injected oocytes (ctrl) or those expressing hTRPV5 WT, mutant A576N, or mutant M577N using a jump protocol, as indicated, in the presence of the DVF extracellular solution. Right: averaged plateau current amplitudes at −100 mV from left panel. NS, not significant. *E*) TRPV5 A576 was replaced by the

(*continued on next page*)

and the *Guide for the Care and Use of Laboratory Animals* (National Institutes of Health, Bethesda, MD, USA).

Electrophysiology with a 2-electrode voltage clamp

The 2-electrode voltage clamp experiments were performed as previously described (38). Briefly, the 2 electrodes (Capillary pipettes; Warner Instruments, Hamden, CT, USA) impaling an oocyte were filled with 3 M KCl to form a tip resistance of 0.3–2 MΩ. Unless otherwise indicated, whole-cell currents of oocytes were recorded at room temperature in standard extracellular solution containing 100 mM NaCl, 2 mM KCl, 1 mM $MgCl_2$, and 10 mM 4-(2-hydroxyethyl)piperazine-1-ethanesulfonic acid (HEPES; pH 7.5). Currents were recorded using a Geneclamp 500B amplifier and Digidata 1322A AD/DA converter (Molecular Devices, Sunnyvale, CA, USA). The pClamp 9 software (Molecular Devices) was employed for data acquisition and analysis. Currents and voltage were digitally recorded at 200 μs per sample and filtered at 2 kHz through a Bessel filter. SigmaPlot 12 (Systat Software, San Jose, CA, USA) was used for data fitting and plotting.

Western blotting and surface protein biotinylation

Xenopus oocytes were washed 3 times with ice-cold PBS solution followed by incubation with 0.5 mg/ml sulfo-NHS-SS-Biotin (Thermo Fisher Scientific, Waltham, MA, USA) for 30 min at room temperature. NH_4Cl (1 M) was used to quench the nonreacted biotin. Oocytes were then washed with ice-cold PBS solution and harvested in ice-cold CelLytic M lysis buffer (Sigma-Aldrich), supplemented with proteinase inhibitor mixture (Thermo Fisher Scientific). Lysates were incubated at 4°C overnight with gentle shaking upon addition of 100 μl streptavidin (Thermo Fisher Scientific). The surface protein absorbed by streptavidin was resuspended in SDS loading buffer and subjected to SDS-PAGE.

Immunofluorescence

Whole-mount immunofluorescence assays using oocytes were performed as previously described (35). Briefly, *Xenopus* oocytes were washed in PBS, fixed in 4% paraformaldehyde for 15 min, washed 3 times in PBS plus 50 mM NH_4Cl, and then permeabilized with 0.1% Triton X-100 for 4 min. Oocytes were then blocked in PBS plus 3% skim milk for 30 min, and then incubated overnight with indicated primary antibodies, followed by incubation with a secondary Alexa Fluor 488–conjugated donkey anti-rabbit antibody (Jackson ImmunoResearch Laboratories, West Grove, PA, USA) for 30 min. Oocytes were then mounted in Vectashield (Vector Laboratories, Burlingame, CA, USA) and examined by AIVI spinning disc confocal microscopy (Cell Imaging Facility, Faculty of Medicine and Dentistry, University of Alberta). The surface expression was assessed by quantifying the plasma membrane immunofluorescence using Volocity 6.2 (PerkinElmer, Waltham, MA, USA).

Mammalian cell electrophysiology

Whole-cell currents were recorded with an EPC9 amplifier (HEKA Elektronik, Lambrecht, Germany) using the Patchmaster software (HEKA). HEK293 cells were transiently transfected with emptor vector from mouse TRPC4α WT or I617N mutant. Experiments were performed 24 h after transfection. Patch pipettes were pulled from borosilicate glass capillaries (Science Products GmbH, Hofheim, Germany) with a PC-10 puller (Narishige International, Setagaya-ku, Tokyo, Japan). Sigmacote (Sigma-Aldrich) was used to coat the pipette tips. The bath solution contained the following (mM): 140 NaCl, 2.8 KCl, 1 $CaCl_2$, 2 $MgCl_2$, 10 HEPES, and 10 glucose (pH 7.2; adjusted with NaOH). Patch pipettes were filled with the following (mM): 120 Cs-glutamate, 8 NaCl, 1 $MgCl_2$, 10 Cs-BAPTA, 3.1 $CaCl_2$ (100 nM free Ca^{2+}), and 10 HEPES (pH 7.2; adjusted with CsOH). TRPC4 current was activated upon application of 10 nM englerin A in bath solution. All currents were normalized to the cell size (pA/pF). Single-channel recording of TRPM8 in a cell-attached configuration was performed at room temperature and analyzed as previously described (36). Borosilicate glass pipettes with resistance of 15–20 MΩ were used. Single-channel currents were filtered at 2 kHz and sampled at 10 kHz. The bath solution contained the following (mM): 150 KCl, 1 MgCl2, 5 glucose, and 10 HEPES (pH 7.3; adjusted with KOH). The pipettes were filled with solution containing the following (mM) 150 NaCl, 1 MgCl2, 5 glucose, and 10 HEPES (pH 7.3; adjusted with NaOH).

Statistical analysis

Data were analyzed and plotted using SigmaPlot 12 (Systat Software) and are expressed as means ± SEM.

RESULTS

TRPV6 and TRPV5 gate residues

We replaced each of the 9 human TRPV6 hydrophobic residues in the distal S6 fragment M610-G619 (**Fig. 1*A***) with hydrophilic asparagine (N) and assessed activities of the mutant channels. We measured steady-state currents at −50 mV induced by the addition of 5 mM extracellular Ca^{2+}, which follows a large, transient Cl^- current, mediated by native Ca^{2+}-activated Cl^- channels (Fig. 1*B*), as described before (37, 39). We indeed found that, compared with wild-type (WT) TRPV6, mutants A616N and M617N exhibited drastic 211 ± 22– and 174 ± 19–fold increases, respectively, in the channel activity, whereas other mutant channels behaved like WT or had lower activities (Fig. 1*B*, *C*). In particular, based on rat TRPV6 crystal structure, the methionine at position 618 (M618) was reported to be the gate residue (13), but we found that the activities of the M618N mutant and WT channels were similar. Because oocytes expressing A616N or M617N showed severe sickness at ~2 d after cRNA injection, presumably because of sustained Ca^{2+} and Na^+ entry mediated by the constitutively active mutant, measurements were performed 1 d after injection. By biotinylation and immunofluorescence, we found that these mutations do not significantly affect plasma membrane targeting (Fig. 1*C*, *D*). Because TRPV6-mediated currents induced by 5 mM

amino acid indicated and the averaged currents were obtained as in panel *B* with the mutants shown (n = 15–20 oocytes from ≥3 batches). *F*) TRPV5 M577 was replaced by different amino acid, as indicated; the resulting membrane currents from different mutants were recorded and averaged as in panel *B* (n = 16–22).

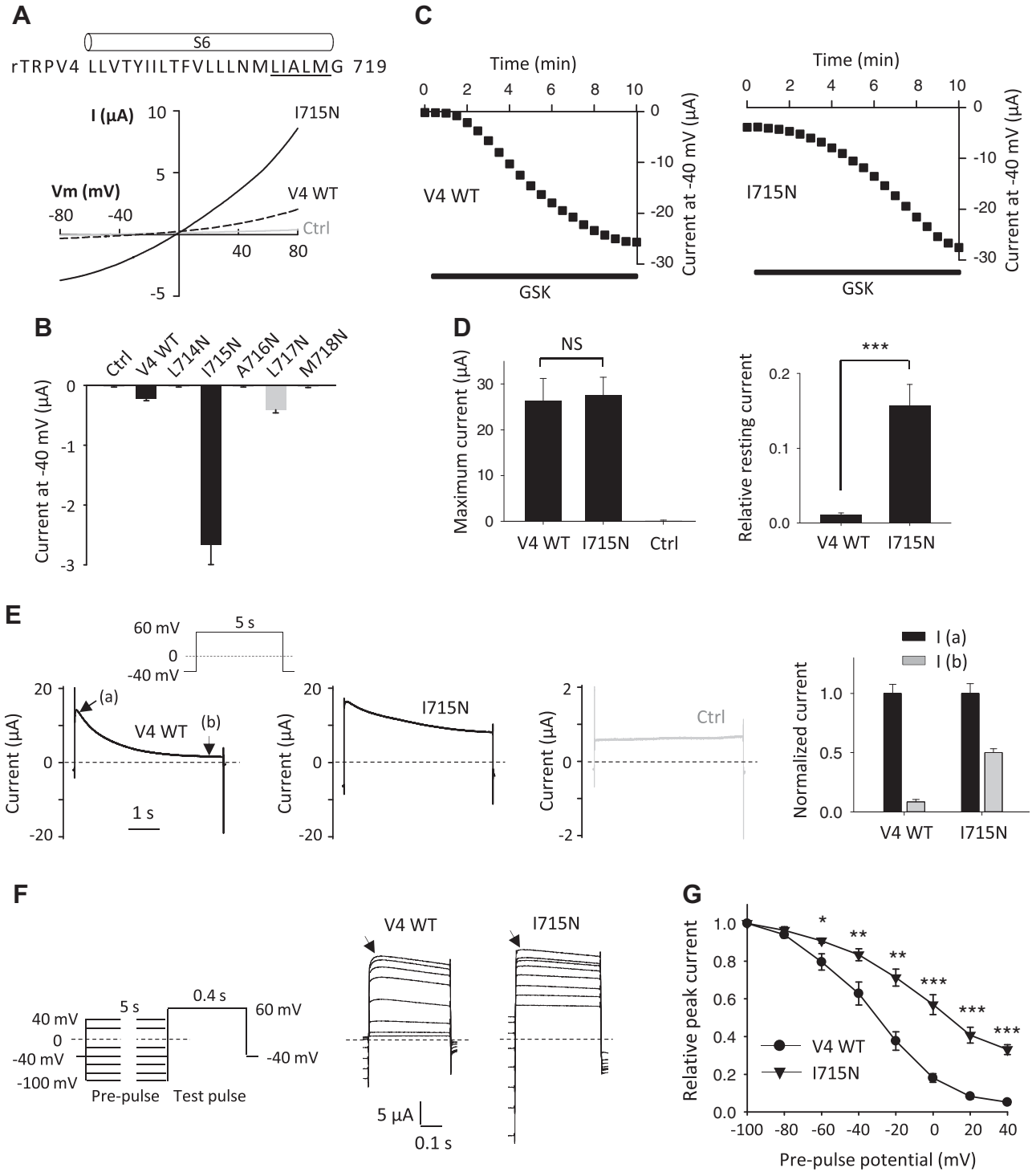

Figure 4. Characterization of point mutants at, and adjacent to, the putative gate region in S6 of rat TRPV4. *A*) Each single underlined amino acid of rat TRPV4 was mutated to N. Representative *I–V* curves were obtained from ctrl (water-injected oocytes), TRPV4 WT, or mutant I715N expressing oocytes in the presence of the Na^+-containing extracellular solution with the following (mM): 100 NaCl, 2 KCl, 1 $MgCl_2$, 10 HEPES (pH 7.5). *B*) Averaged currents at −40 mV obtained under the same experimental conditions as in panel *A* in expressing or control oocytes, as indicated. Currents were averaged from 14 to 18 oocytes of ≥3 batches. *C*) Representative currents at −40 mV as a function of time over 10 min after 100 nM GSK was added in oocytes expressing TRPV4 WT or I715N mutant. Currents were recorded every 30 s using a ramp protocol as in panel *A*, and data at −40 mV were extracted for the presentation. *D*) Averaged maximal currents and ratios of the resting current to the current induced by 100 nM GSK at −40 mV in oocytes expressing TRPV4 WT or mutant I715N under the same experimental conditions as shown in panel *C*. Ctrl, water-injected oocytes. NS, not significant. ***$P < 0.001$. *E*) Left: representative traces showing channel inactivation at a holding depolarization of +60 mV for 5 s, in oocytes expressing TRPV4 WT or mutant I715N or water-injected oocytes (ctrl) in the same Na^+-containing solution as in panel *A* plus 5 mM $CaCl_2$. Right: Averaged and normalized currents at the peak (*a*) or steady state (*b*), as indicated in the left panel. Background current from ctrl was subtracted. *F*) Voltage dependence

(*continued on next page*)

extracellular Ca^{2+} may still contain some residual Ca^{2+}-induced Cl^- current at the plateau, we also preinjected 25 nl of 50 mM EGTA into each oocyte 2 h before current measurements and found that mutants A616N and M617N still showed similar, dramatic increases in channel activity compared with WT TRPV6 (Fig. 1*E*). In the presence of divalent-free (DVF) extracellular solution, TRPV6 is known to be constitutive open at negative voltages (40). Interestingly, we found that under that ionic condition, the A616N or M617N mutation had little effect on the TRPV6-mediated monovalent currents at negative voltages (Fig. 1*F, G*), suggesting the absence of a hydrophobic gating when TRPV6 channels are already in an open state. Because both intra- and extracellular Ca^{2+} are known to induce partial channel inactivation in TRPV6 (41), we next wanted to know whether the large Ca^{2+}-induced currents observed in A616N and M617N mutants (Fig. 1*C, E*) were due to reduced Ca^{2+}-induced inactivation. We compared WT and mutant TRPV6 in the simultaneous presence of extracellular Na^+ and Ca^{2+}. To minimize the effect of changes in the intracellular Ca^{2+} concentration and contaminations by endogenous Cl^- currents, we performed electrophysiologic measurements at −30 mV in oocytes preinjected with EGTA and bathed in Na^+-containing extracellular solution ± 5 mM $CaCl_2$. We found that, although Ca^{2+} inhibited Na^+ currents mediated by WT TRPV6, the Ca^{2+}-induced inhibition in oocytes expressing A616N or M617N was only temporary and was followed by large increases in the inward current (Fig. 1*H*), suggesting that the pore cannot be effectively closed during the Ca^{2+}-induced inactivation in the A616N or M617N mutant. Further, when we replaced each hydrophobic residue in fragment M610-G619 with the hydroxyl-containing serine (S), we found similar drastic increases in the channel activity for A616S and M617S mutants but not for any of the other serine mutants (Fig. 1*I*). Thus, these data together indicated that A616 and M617 act as gate residues.

We next replaced A616 with 10 aa residues of different hydrophobicities and/or sizes (Supplemental Table 1) and found that mutation to a bulky and hydrophobic amino acid (V, I, F, Y, or W) abolished the channel activity, whereas replacement with a small or hydrophilic amino acid (G, T, S, Q, or N) tremendously increased the channel activity (**Fig. 2*A***), which is in strong agreement with the hydrophobic theory. Replacement of M617 by different amino acids, in general, produced similar results as those for A616 (Fig. 2*B*). The mutations at A616 and M617 did not affect TRPV6 targeting to the surface membrane (Fig. 2*C* and Supplemental Fig. S2*A*) as assayed by biotinylation and immunofluorescence. So far, our results have shown that both A616 and M617 act as the hydrophobic gate residues. A noticeable difference between the 2 sites was that replacement of M617 with smaller residues A or G did not increase the activity, whereas replacement of A616 with G substantially increased the activity (Fig. 2*A, B*), suggesting that, compared with M617, A616 is a more primary gate residue. Next, we examined double mutants with each carrying 2 very different mutations (one to hydrophilic N and the other to large hydrophobic W)—A616N/M617W and A616W/M617N—which are "mirror symmetrical" to each other (*i.e.*, NW *vs.* WN), and found that mutant A616N/M617W still exhibited a substantial activity increase, whereas A616W/M617N was nonfunctional (Fig. 2*D*), even though they both exhibited similar surface-membrane expression (Supplemental Fig. S2*B, C*). In other words, the pore can be closed at site 616 (by changing to W), regardless of what happens at site 617, but not *vice versa*. These results were in strong support of an "asymmetric" arrangement; in which, A616 points more toward the pore center than M617 does and, thus, acts as the primary gate, whereas M617 is, rather, a secondary gate residue.

Because TRPV5 is a close homolog of TRPV6 and shares 75% amino acid identity with TRPV6, we next wanted to determine whether TRPV5 contained the same gate signature as TRPV6. Through replacing each of the hydrophobic residues in the F574–M578 fragment (corresponding to TRPV6 L614-M618 containing the gate) with N, we found that, similar to TRPV6, either mutant A576N or M577N, but not any of the other mutants, exhibited the tremendously increased channel activity, compared with WT TRPV5, whereas these mutations did not affect plasma membrane expression (**Fig. 3*A, B***). When oocytes were preinjected with EGTA 2 h before current measurements, mutant channels A576N and M577N also showed similar increases in the channel activity as WT TRPV5 (Supplemental Fig. S3). Like TRPV6, TRPV5 showed little changes in the monovalent current at hyperpolarized voltages in the presence of the DVF solution when the A576N or M577N mutation was introduced (Fig. 3*C, D*). When A576 or M577 was replaced by amino acid residues of various hydrophobicities and/or sizes, TRPV5 channel activity exhibited strong correlation with the residue's hydrophilicity at either the 576 or 577 site (Fig. 3*E, F*). These data indicated that TRPV5 possesses conserved gate residues A576 and M577, corresponding to those of TRPV6.

TRPV4 gate residue

In contrast to TRPV6 and TRPV5, the analogous asparagine mutations in the distal S6 fragment L714-M718 of TRPV4 revealed that only mutant I715N exhibits substantially increased channel activity (**Fig. 4*A, B***), suggesting

of channel inactivation. Left: voltage jump protocol, showing voltage holding for 5 s at various values in the −100 to +40 mV range, at 20 mV increments, followed by voltage holding at +60 for 0.4 s to provide a channel-activity readout. Middle and right: under the same ionic conditions as in panel *E*, representative current traces right after voltage holdings for 5 s, showing peak currents, as indicated by the arrows. *G*) Averaged and normalized peak currents at +60 mV obtained from experiments in panel *F*, showing the voltage dependence of channel inactivation of WT TRPV4 ($n = 7$) and mutant I715N ($n = 9$). $^*P < 0.05$, $^{**}P < 0.01$, $^{***}P < 0.001$.

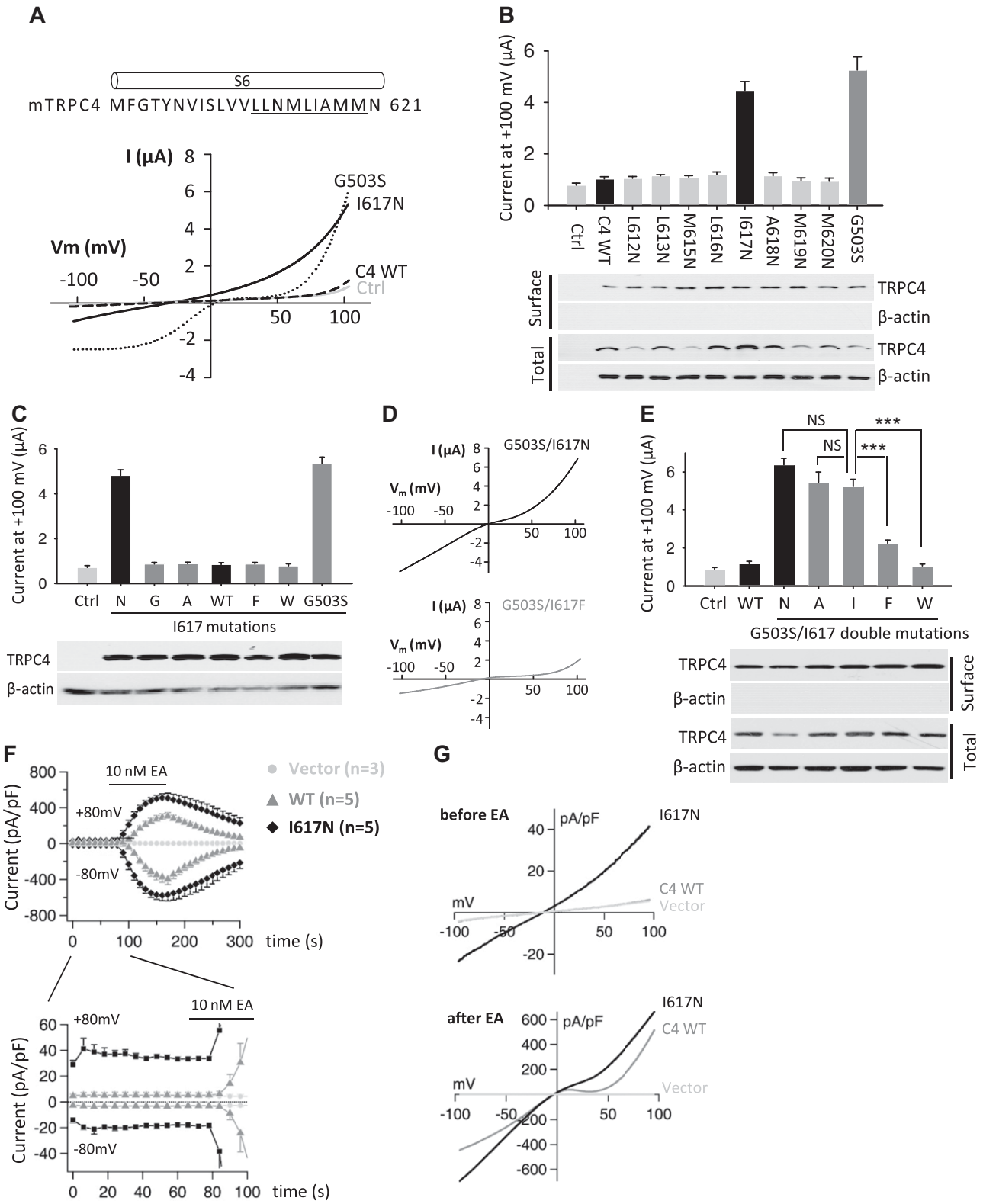

Figure 5. Characterization of mouse TRPC4 point mutants at, and adjacent to, the putative gate region in S6. *A*) Each single, underlined amino acid of TRPC4 was mutated to N. Representative *I–V* curves were obtained in oocytes expressing TRPC4 WT, mutants I617N or G503S, or water-injected oocytes (Ctrl), in the presence of the Na^+-containing extracellular solution with the following (mM): 100 NaCl, 2 KCl, 1 $MgCl_2$, 10 HEPES (pH 7.5). The gain-of-function mutant G503S (within the S4–S5 linker) serves as a positive control. *B*) top: averaged currents obtained at +100 mV under the same condition as in panel *A* for oocytes expressing one of the asparagine mutants, as indicated (n = 18–21). Bottom: Western blot of surface-biotinylated and total protein of TRPC4 WT or mutants. *C*) Top: averaged currents for TRPC4 WT or G503S or I617 mutants, as indicated (n = 15–21). Bottom: Western blot showing total protein of TRPC4 WT or an indicated mutant expressed in oocytes. *D*) Representative *I–V*

(*continued on next page*)

that the TRPV4 gate is composed of a single hydrophobic residue. Of note, the A716 and L717 sites that correspond to the A616/M617 gate in TRPV6 and the A576/M577 gate in TRPV5 did not give rise to greater channel activity. GSK is a known chemical agonist of TRPV4, which substantially increases the channel open probability (42). We next tested the effects of GSK on WT TRPV4 and mutant I715N channels and found that, at a saturated concentration (100 nM), GSK further increased the mutant's channel activity (Fig. 4*C*), suggesting that the I715N mutant might not be in a fully open state and can be further opened by an agonist. Interestingly, the I715N mutant exhibited similar GSK-induced maximal currents as WT channels (Fig. 4*C, D*), indicating that the gate mutant I715N has a similar maximal channel activity as WT channel has, a property shared by TRPV6 and TRPV5 (Figs. 1*G* and 3*D*). Because of much lower WT channel activity compared with mutant I715N in the absence of an agonist, the ratio of the resting current to the GSK-activated current was much smaller in the WT channel than it was in the I715N mutant (Fig. 4*D*). In other words, GSK induced much larger fold increases in the channel activity of the WT channel than the mutant I715N did. We also performed noise analysis on whole-cell current traces obtained at −100 mV and found that, in the absence of an agonist mutant, I715N has much higher open probability values than WT TRPV4 has (0.41 ± 0.07 *vs.* 0.06 ± 0.02, $n = 4$), whereas their single-channel currents were comparable (7.4 ± 1.1 *vs.* 5.3 ± 0.9, $n = 4$). These data together indicate that I715 acts as an activation gate in TRPV4.

We next wanted to determine whether the same gate was involved in TRPV4 channel inactivation induced by prolonged depolarization, which was previously reported (43). Indeed, although depolarization at +60 mV for 5 s resulted in significant current decay for WT TRPV4, it had a much more moderate effect on gate mutant I715N (Fig. 4*E*), suggesting that I715 also serves as the inactivation gate. We also examined the voltage dependence of the inactivation by holding the membrane potential at each of the different values in the −100 to +40 mV range for 5 s and measuring the peak current at +60 mV right after each voltage holding, as previously used (43). We found that the gate mutant exhibits greatly reduced channel inactivation in the −60 to +40 mV range (Fig. 4*F, G*).

TRPC4 and TRPM8 gate residues

To study whether members of the TRPC and TRPM subfamilies possess a single- or double-residue gate, we examined TRPC4 and TRPM8. TRPC4 is activated by stimulation of GPCRs, and the resulting currents are doubly (outwardly and inwardly) rectifying (44). We reasoned that an appropriate mutation to the gate residues must constitutively open the channel and produce detectable currents without receptor activation. We replaced each of the 9 residues around the putative gate residues, L612–M620 (**Fig. 5*A***), with N in mouse TRPC4 and studied their channel activities in oocytes. We found that mutant I617N, but not WT or any other mutant channels, produced a current as large as that reported by gain-of-function mutant G503S, which is trapped in a constitutively activated state (33) (Fig. 5*A, B*), suggesting the presence of a single-residue gate. Of note, *I–V* curves for the 2 mutants I617N and G503S were characteristically different (Fig. 5*A*), probably because they are opened by 2 very different processes (see below). With biotinylation and immunofluorescence, we found that the plasma membrane localization of these mutants was similar to that of the WT channel (Fig. 5*B* and Supplemental Fig. S4*A*). Replacement of I617 by A, G, F, or W did not result in any appreciable current (Fig. 5*C*). Further, on top of the G503S mutation, replacement of I617 by the large hydrophobic residue F or W, but not A or N, resulted in significantly decreased channel activity (Fig. 5*D, E*). When expressed in HEK293 cells, the TRPC4 I617N mutant, but not the WT channel, produced appreciable currents in the absence of an agonist (Fig. 5*F* and Supplemental Fig. S5*B*) and exhibited an *I–V* curve similar to that obtained from using *Xenopus* oocytes (Fig. 5*A, G*, top panel). These data supported our conclusion drawn from using oocyte electrophysiology that TRPC4 possesses a single-residue gate I617. Similar to TRPV4 I715N mutant, the TRPC4 I617N mutant can also be further activated by its agonist englerin A (45) (Fig. 5*F, G*, bottom panel). Agonist-induced channel activation is believed to accompany conformational changes in the protein that leads to gate residue movements, resulting in the opening of the pore. In comparison, pore opening through direct hydrophilic substitution at the gate site would not be associated with similar conformational changes. We thus think that those constitutive open gate mutants should still be in a resting (nonactivated) state. Consistently, TRPC4 channel activated by either englerin A or the G503S mutation gave rise to doubly rectifying *I–V* curves (Fig. 5*A, G*, bottom panel), which were not seen in the gate mutant I617N (Fig. 5*A, G*, top panel).

TRPM8 is a cold-sensitive channel and is activated by cooling agents, such as menthol (46). In oocytes, TRPM8 produced voltage-dependent activation currents with pronounced outward rectification (**Fig. 6*A***), in line with previous report that TRPM8 is closed by a voltage-dependent mechanism at negative membrane potentials (47). We reasoned that hydrophilic substitutions of the hydrophobic gate residues must constitutively open the pore and thus give rise to detectable currents at negative

curves for G503S/I617N and G503S/I617F double mutants, obtained under the same experimental condition as in panel *A*. *E*) Top: averaged currents at +100 mV for different G503S/I617 double mutants, as indicated ($n = 14$–20). Bottom: Western blot of surface biotinylated and total protein of indicated mutants expressed in oocytes. NS, not significant. $^{***}P < 0.001$. *F*) Whole-cell outward (+80 mV) and inward (−80 mV) current recordings in HEK293 cells transiently transfected with vector-only as the control (black circle), TRPC4 WT (blue), or the I617N mutant cDNAs (purple). TRPC4-mediated current was activated upon application of 10 nM englerin A at the time point indicated. Shown are mean currents plotted *vs.* time. *G*) Representative *I–V* curves obtained as in panel *F* before (top) and after (bottom) englerin A application (for peak currents).

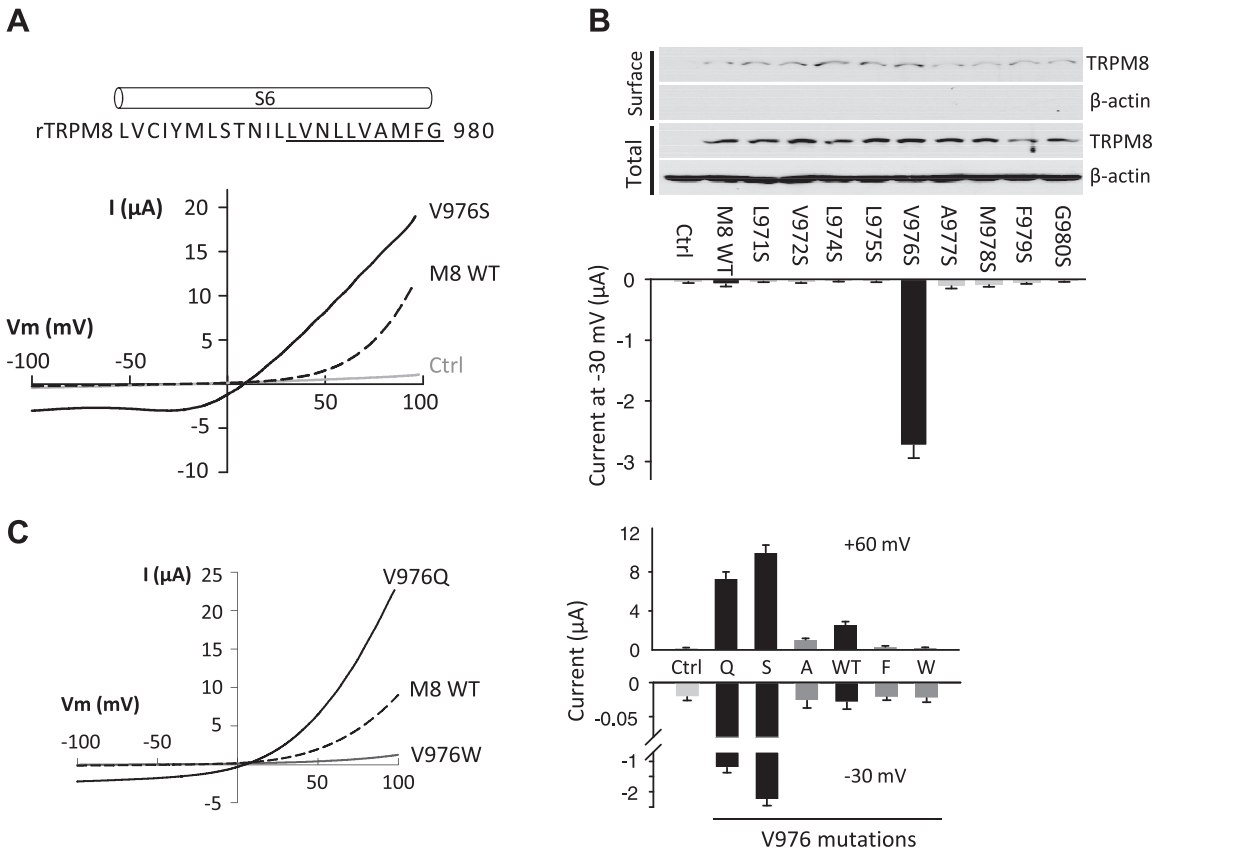

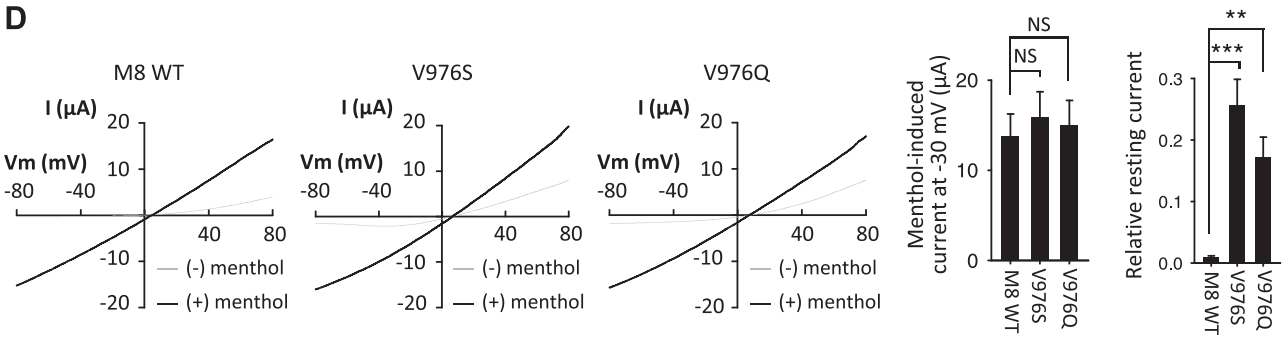

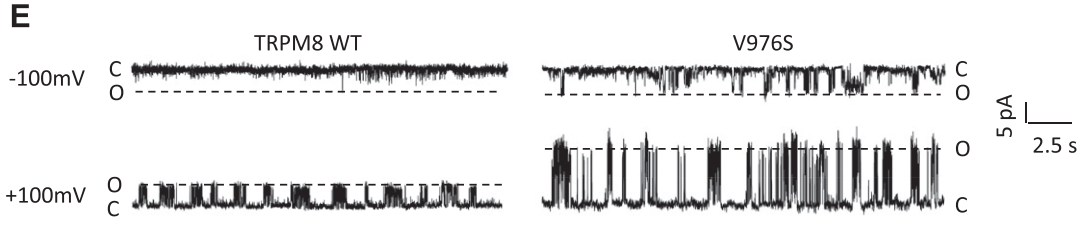

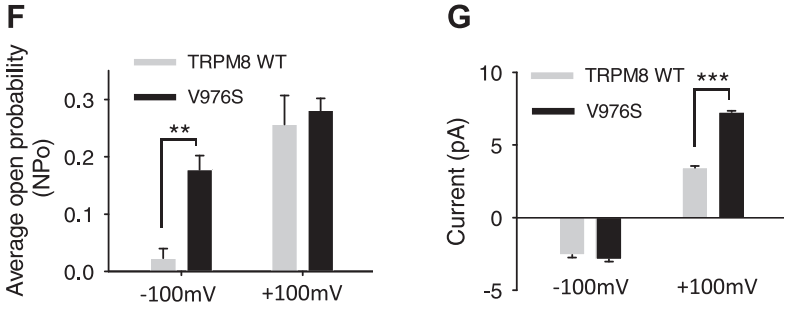

(*continued on next page*)

voltages. Based on the S6 alignment (Supplemental Fig. S1), we mutated each of the 9 individual hydrophobic residues between L971 and G980 to serine (Fig. 6*A*) and found that, in the absence of menthol V976S, but not the WT or any other mutant channels, produced robust currents at negative voltages (Fig. 6*A, B*, bottom panel). Consistently, mutant channel V976S showed moderately increased currents at positive voltages under our experimental condition (Supplemental Fig. S5*A*). Biotinylation assays showed that all tested TRPM8 mutants have similar surface expression as that of WT (Fig. 6*B*, top panel). Replacing V976 with Q produced comparable large activities as that produced by V976S (Fig. 6*C*), but replacements with the large hydrophobic residues F and W, abolished the channel activity (Fig. 6*C*). We also applied 2.5 mM menthol to fully activate TRPM8 channel (48) and found that, although mutants V976S and V976Q showed similar menthol-induced maximal currents as the WT channel had (Fig. 6*D*), the mutant channels exhibited a much larger ratio of resting current to the menthol-activated current (Fig. 6*D*), a property shared by TRPV4 (Fig. 4*C, D*). In summary, our studies showed that V976 acts as the single-residue gate for TRPM8.

We also examined single-channel activity of the V976S mutant in HEK293 cells by patch clamp recordings. Transient expression of mutant V976S in HEK293 cells led to increased cell death at 48 h posttransfection (Supplemental Fig. S5B), probably because of Ca^{2+} overload through constitutive channel activity. At 24 h after transfection, the V976S mutant channel's open probability was substantially increased at −100 mV, whereas the single-channel current was not affected, when compared with WT TRPM8 (Fig. 6*E–G*). Replacement of V976 with a hydrophilic residue, such as S, presumably resulted in an increased hydration rate of the channel pore, thereby substantially increasing the channel open probability. In contrast, at +100 mV, the V976S mutation did not increase the open probability (Fig. 6*E, F*), probably because the open probability of WT TRPM8 already reached its maximum under this condition because strong depolarization, such as +100 mV, is known to activate the WT TRPM8 channel (47). Interestingly, the V976S mutation substantially increased the single-channel current at +100 mV (Fig. 6*E, G*), possibly because, at +100 mV, the V976S mutation removed the hydrophobic gate seal, which increased the hydrophilicity of the gate region to allow intracellular cations (K^+) to accumulate in the vestibule between the lower gate and the selectivity filter, thereby increasing the supply of cation efflux from the vestibule to the extracellular milieu. At negative potentials, the mutation did not influence the cation influx because of an unaffected supply of extracellular cations (Na^+). A similar mechanism was previously reported to account for the large, single-channel conductance of BK potassium channels (49).

DISCUSSION

In this study, we functionally identified hydrophobic gate residues in the cytoplasmic end of S6 in 5 TRP channels from 3 TRP subfamilies. Although we identified we identified a conventional single amino-acid gate residue in TRPV4, TRPC4, and TRPM8, we found that in TRPV6 and TRPV5, 2 consecutive amino acids together formed a double-residue gate. All identified gate residues were within the gate motif $YX_1X_2X_3X_4X_5X_6Y$ in the distal S6 (**Fig. 7*A*** and Supplemental Fig. S1), with a cluster of hydrophobic residues (X_1–X_6) surrounded by 2 hydrophilic residues (Y). The X_3 in the gate motif was identified as a gate site in the majority of all studies, including the reported structural studies (12, 13, 15–17, 50).

The residues M618 in TRPV6 (13) and M645 in TRPV2 (12), identified as gates by the structural analysis, align well with each other, but right beside the TRPV6 gate A616-M617 identified by our functional studies (Fig. 7*A*). In contrast, the TRPV1 gate L681 identified by the functional SCAM (50) corresponds exactly to the TRPV6 secondary gate M617 identified in our study (*i.e.*, the X_5 in the gate motif). Apparently, TRPV configurations under experimental conditions in the functional studies may be different from those in structural analyses. The fact that the TRPV1, TRPV2, and TRPV6 lower gates predicted from the structures (Fig. 7*A*) do not align could be caused by distinct properties of the 3 highly homologous, but not identical, proteins or the experimental conditions used to elucidate the structures [*i.e.*, conditions used in cryo-EM (TRPV1, TRPV2) or crystallography (TRPV6)].

Hydrophilic substitution at hydrophobic gate residues of TRP channels, which removes the gate seal, has distinct

Figure 6. Characterization of rat TRPM8 point mutants at and adjacent to the putative gate region in S6. *A*) Each single underlined amino acid of TRPM8 was replaced by serine (S). Representative *I–V* curves were obtained in oocytes expressing TRPM8 WT or its mutant V976S or water-injected oocytes (ctrl) at room temperature in the presence of the Na^+-containing extracellular solution with the following (mm): 100 NaCl, 2 KCl, 1 $MgCl_2$, 10 HEPES at pH 7.5. *B*) Top: Western blot of surface biotinylated and total protein of TRPM8 WT or an indicated mutant or water-injected oocytes (ctrl). Bottom: averaged currents obtained at −30 mV from panel *A* (n = 16–21). *C*) Left: representative *I–V* curves obtained from oocytes expressing TRPM8 WT, V976Q mutant, or V976W mutant as in panel *A*. *Right:* averaged currents at −30 and +60 mV under the same condition as in the left panel in oocytes expressing TRPM8 WT or indicated V976 mutants (n = 18–22). *D*) Left: representative *I–V* curves obtained in oocytes expressing TRPM8 WT, mutant V976S, or mutant V976Q at room temperature in the presence of the same Na^+-containing extracellular solution as in panel A, without (−) or with (+) 2.5 mM menthol. Rght: averaged maximal currents and ratios of the resting current to the current induced by 2.5 mM menthol at −30 mV in oocytes expressing TRPM8 WT, mutant V976S, or mutant V976Q under the same experimental conditions as in the left panel. NS, not significant. $^{**}P < 0.01$, $^{***}P < 0.001$. *E*) Representative single-channel recordings of TRPM8 WT and V976S mutant transiently expressed in HEK293 cells under the cell-attached configuration at clamped voltages indicated. C and O indicate the closed and open states, respectively. *F, G*) Averaged channel open probabilities and current amplitudes obtained from single-channel recordings of ~30-s duration. TRPM8 WT (n = 3) and V976S (n = 3). $^{**}P < 0.01$, $^{***}P < 0.001$.

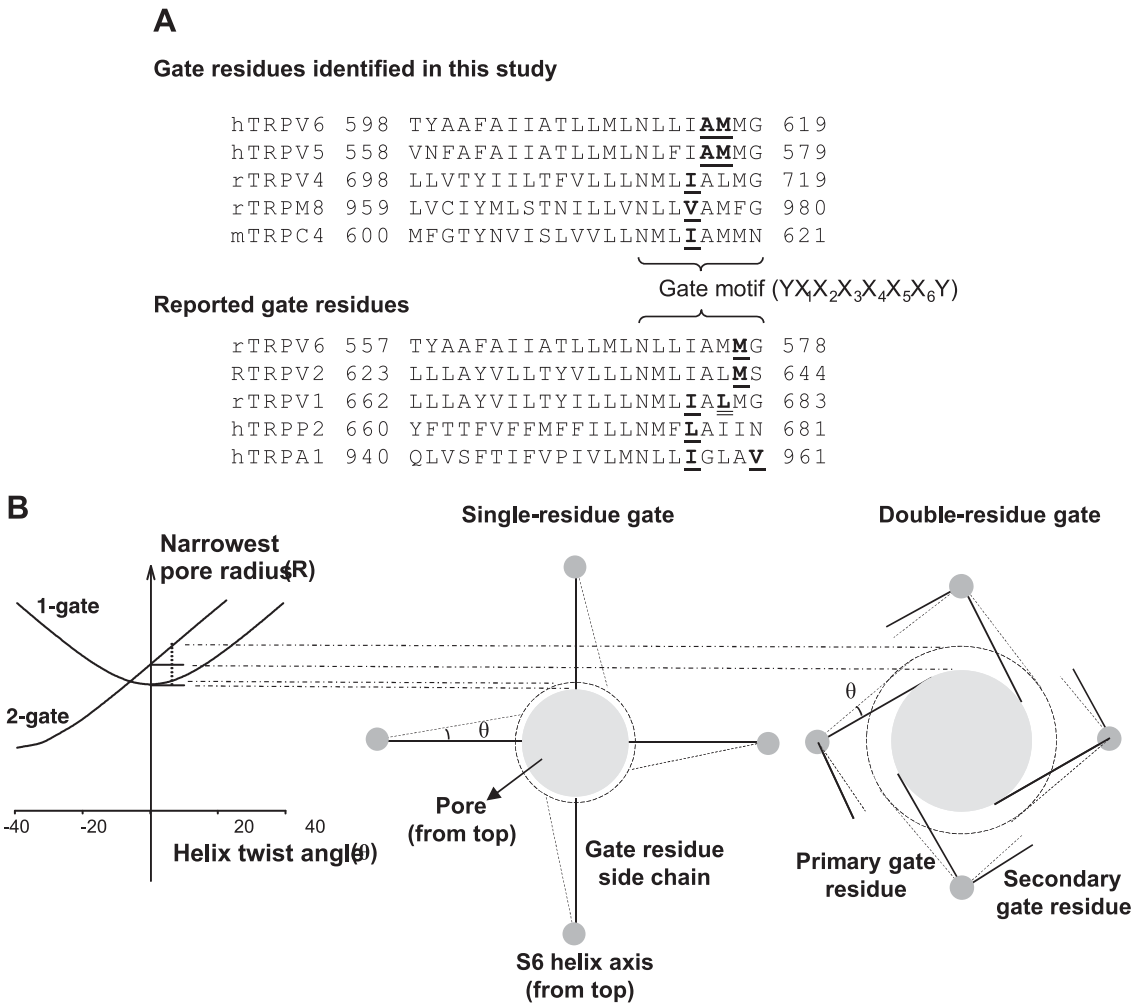

Figure 7. Summary of identified gate residues and twisting models of gate residues upon channel activation. *A*) Top: alignment of the S6 helix sequences of the 5 TRP channels studied here. Identified gate residues are bold and underlined with the $YX_1X_2X_3X_4X_5X_6Y$ motif indicated in which the Y is a hydrophilic residue, and X is a hydrophobic residue. Bottom: alignment of the S6 helix sequences of the 5 TRP channels whose structures were recently solved [TRPV6 (13), TRPV2 (12), TRPV1 (15), TRPP2 (17), and TRPA1 (16)]. Identified gate residues are bold and underlined. The gate residue identified by SCAM in TRPV1 is bold and double underlined (50). h, human; m, mouse; r, rat; R, rabbit. First and last amino acid numbers are indicated. *B*) Pore size changes in single- and double-residue gate models after helix twist. *B*t) Left: narrowest pore radius (*R*, arbitrary unit) as a function of the helix twist angle (θ) according to $R = \mathrm{Sqrt}[R_0^2 + 2A(A + R_0)(1 - \cos\theta)] = \mathrm{Sqrt}[9 + 176 \times (1 - \cos\theta)]$, where R_0 and A, the initial pore radius (when θ = 0) and gate amino acid length were assumed to be 3 and 8 nm, respectively. This relationship holds true when twist angles remain small, so that only the (primary) gate residue is involved in defining the pore size. Middle: schematic illustration of a single-residue gate model in which the pore size increases when helices twist in a small counterclockwise angle. S6 helix axes are marked by small gray circles. Large gray and dashed line circles represent the narrowest pore before and after twisting, respectively. Gate residue side chains before and after twisting are indicated by solid and dashed lines, respectively. Right: double-residue gate model in which the primary and secondary gate amino acids are, respectively, indicted by long and short lines, which were assumed in the drawing to form an angle of 40 and 60°, respectively, with the line linking the helix center and pore center.

effects, depending on the states of the channels. When TRP channels were in low-activity states, the hydrophilic substitution substantially increased the activity of the TRP channels (Figs. 1*C*, 3*B*, 4*B*, 5*B*, and 6*B*). In contrast, when TRP channels were in activated states (*i.e.*, by a chemical agonist, depolarization, hyperpolarization, constitutively activating mutation, or a removal of an inhibitor), the hydrophilic substitution can no longer further increase the channel activity (*i.e.*, WT and mutant channels have similar maximal activated currents) (Figs. 1*G*, 3*D*, 4*D*, 5*E*, and 6*D*). These data may have revealed some profound differences among channel openings by an "agonist" and direct removal of the gate seal (by hydrophilic substitution in our study). We think that hydrophilic substitution of the gate residues represents gate opening and other changes that are mainly local to the gate site and that, in contrast, an agonist induces more global conformational changes that include gate opening and other relevant changes along the pore (*i.e.*, the selectivity filter). That would suggest that an agonist may induce a much larger pore opening than the hydrophilic substitution of gate residues, which is supported by our observations in TRPV4 and TRPM8 that chemical agonists GSK and menthol still induced large increases in the activity of their gate mutants (Figs. 4C and

6*D*). Although the concept of single-residue gate has been generally accepted, some bacterial ion channels were reported to possess a double-residue gate in which the 2 residues are 1 turn away from each other (26, 27), which is similar to the TRPA1 gate indicated by a structural study (16) (Fig. 7*A*). For TRPV4, TRPM8, and TRPC4 channels, the single-gate residue presumably faces the pore. We propose a model in which the 4 gate residues in a tetramer define the narrowest pore constriction (Fig. 7*B*, middle panel). In contrast, for TRPV6 and TRPV5, which possess a double-residue gate, either of the 2 gate residues would face away from the pore axis (Fig. 7*B*, right panel). In this model, the primary gate residue was drawn to face slightly more toward the pore center than the secondary gate residue, to reflect their different sensitivities to small changes in the residue hydrophobicity and size. In fact, unlike primary gate residues, substitutions of a secondary gate residue in TRPV6 or a single-gate residue in TRPC4 and TRPM8 to an amino acid among A, V, I, and L did not give rise to appreciable changes in the channel activity (Figs. 2*B*, 5*C*, and 6*C*).

Gating of an ion channel may involve complex protein conformational changes, which may include a combination of S6 splaying, twisting, and bending. Unlike potassium channels that possess a canonical S6 PVP motif to allow helix bending (25), TRP channels do not have a similar PVP motif in their S6 and thus are not likely to be involved in an S6 bending movement. Interestingly, structures of human TRPP2 in various states revealed a rotational twist in the S6 gate region, leading to pore dilation (18). By SCAM analysis, using extracellular thiol-modifying compounds, the TRPV5 upper gate (selectivity filter) was also shown to undergo pH-dependent twisting (29). We propose models here to illustrate pore opening and closing through twisting of the 4 S6 helices around their axes in the TRP channels with a single- or double-residue gate (Fig. 7*B*). These models show that a double-residue gate allows much more efficient changes in pore size than a single-residue gate does, through twisting of the same angle (Fig. 7*B*), which represents a unique characteristic of double-residue gate channels. Thus, it would be interesting to see whether, under physiologic conditions, TRP channels with double-residue gates are associated with smaller gate conformational changes as compared with those with a single-residue gate.

It would be worthy to speculate possible functional roles of the 2 hydrophilic residues located at the 2 ends of the gate motif $YX_1X_2X_3X_4X_5X_6Y$. We notice that they have a distance of 6 aa, which represents about 2 helical turns and that the X_3 site, located roughly in the middle, was identified as the gate residue in most TRP channels presently studied or previously reported. This would mean that the gate residue is sandwiched by the 2 hydrophilic residues and that all residues may face the pore, to unambiguously and efficiently define the hydrophobic gate residue. That hydrophilic–hydrophobic–hydrophilic arrangement would ensure that only the hydrophobic residue would always control the pore opening and closing.

In summary, we have identified distinct amino acid residues within the gate motif of the distal part of the pore-lining S6 helix, which form the most constricted sites of the lower gate in TRPV6 and TRPV5 (double-residue gate) and in TRPV4, TRPM8, and TRPC4 (single-residue gate). By use of agonists, we performed biophysical analyses on these gain-of-function gate mutants and revealed shared gating properties that are distinct from those of WT TRP channels. We found that a double-residue gate channel is more sensitive than a single-residue gate channel to small changes in the hydrophobicity and/or size of the gating residues, as it is to S6 helix twisting. Single- and double-residue gating may have been evolutionarily adapted by TRP channels to respond to a variety of physiologic stimuli that induce distinct gate conformational changes associated with channel opening and closing. FJ

ACKNOWLEDGMENTS

The authors are grateful to J. Y. Lapointe (University of Montreal, Montreal, QC, Canada) for valuable comments and X. Liu (University of Alberta) for important contributions to electrophysiology experiments. This work was supported by the Natural Sciences and Engineering Research Council of Canada (NSERC; to X.-Z.C.), the National Natural Science Foundation of China (Grant 81570648, to X.-Z.C.and 81602448, to J.T.), and by the Deutsche Forschungsgemeinschaft (DFG;, Sonderforschungsbereich/Transregio 152, to V.F.). W.Z. was a recipient of the Alberta Innovates–Doctoral Graduate Student Scholarship. R.C. and Q.H. were recipients of the NSERC International Research Training Group (IRTG) Studentship. L.H. was a recipient of the IRTG 1830 Student Scholarship (DFG). The authors declare no conflicts of interest.

AUTHOR CONTRIBUTIONS

W. Zheng, J. Tang, P. Light, V. Flockerzi, Y. Cao, and X.-Z. Chen conceptualized the study; W. Zheng, R. Hu, R. Cai, L. Hofmann, Q. Hu, M. Fatehi, W. Long, T. Kong, and J. Tang performed the investigations; and W. Zheng, V. Flockerzi, and X.-Z. Chen wrote the paper.

REFERENCES

1. Clapham, D. E. (2003) TRP channels as cellular sensors. *Nature* **426**, 517–524
2. Julius, D. (2013) TRP channels and pain. *Annu. Rev. Cell Dev. Biol.* **29**, 355–384
3. Ishimaru, Y., and Matsunami, H. (2009) Transient receptor potential (TRP) channels and taste sensation. *J. Dent. Res.* **88**, 212–218
4. Eijkelkamp, N., Quick, K., and Wood, J. N. (2013) Transient receptor potential channels and mechanosensation. *Annu. Rev. Neurosci.* **36**, 519–546
5. Montell, C. (2005) The TRP superfamily of cation channels. *Sci. STKE* **2005**, re3
6. Clapham, D. E., Runnels, L. W., and Strübing, C. (2001) The TRP ion channel family. *Nat. Rev. Neurosci.* **2**, 387–396
7. Liu, C., and Montell, C. (2015) Forcing open TRP channels: mechanical gating as a unifying activation mechanism. *Biochem. Biophys. Res. Commun.* **460**, 22–25
8. Nilius, B., Owsianik, G., Voets, T., and Peters, J. A. (2007) Transient receptor potential cation channels in disease. *Physiol. Rev.* **87**, 165–217
9. Nilius, B., Voets, T., and Peters, J. (2005) TRP channels in disease. *Sci. STKE* **2005**, re8
10. Shapovalov, G., Ritaine, A., Skryma, R., and Prevarskaya, N. (2016) Role of TRP ion channels in cancer and tumorigenesis. *Semin. Immunopathol.* **38**, 357–369

11. Moran, M. M., McAlexander, M. A., Bíró, T., and Szallasi, A. (2011) Transient receptor potential channels as therapeutic targets. *Nat. Rev. Drug Discov.* **10**, 601–620
12. Zubcevic, L., Herzik, M. A., Jr., Chung, B. C., Liu, Z., Lander, G. C., and Lee, S. Y. (2016) Cryo-electron microscopy structure of the TRPV2 ion channel. *Nat. Struct. Mol. Biol.* **23**, 180–186
13. Saotome, K., Singh, A. K., Yelshanskaya, M. V., and Sobolevsky, A. I. (2016) Crystal structure of the epithelial calcium channel TRPV6. *Nature* **534**, 506–511
14. Huynh, K. W., Cohen, M. R., Jiang, J., Samanta, A., Lodowski, D. T., Zhou, Z. H., and Moiseenkova-Bell, V. Y. (2016) Structure of the full-length TRPV2 channel by cryo-EM. *Nat. Commun.* **7**, 11130
15. Liao, M., Cao, E., Julius, D., and Cheng, Y. (2013) Structure of the TRPV1 ion channel determined by electron cryo-microscopy. *Nature* **504**, 107–112
16. Paulsen, C. E., Armache, J. P., Gao, Y., Cheng, Y., and Julius, D. (2015) Structure of the TRPA1 ion channel suggests regulatory mechanisms. *Nature* **520**, 511–517
17. Shen, P. S., Yang, X., DeCaen, P. G., Liu, X., Bulkley, D., Clapham, D. E., and Cao, E. (2016) The structure of the polycystic kidney disease channel PKD2 in lipid nanodiscs. *Cell* **167**, 763–773.e11
18. Wilkes, M., Madej, M. G., Kreuter, L., Rhinow, D., Heinz, V., De Sanctis, S., Ruppel, S., Richter, R. M., Joos, F., Grieben, M., Pike, A. C., Huiskonen, J. T., Carpenter, E. P., Kühlbrandt, W., Witzgall, R., and Ziegler, C. (2017) Molecular insights into lipid-assisted $Ca2^{+}$ regulation of the TRP channel Polycystin-2. *Nat. Struct. Mol. Biol.* **24**, 123–130
19. Grieben, M., Pike, A. C., Shintre, C. A., Venturi, E., El-Ajouz, S., Tessitore, A., Shrestha, L., Mukhopadhyay, S., Mahajan, P., Chalk, R., Burgess-Brown, N. A., Sitsapesan, R., Huiskonen, J. T., and Carpenter, E. P. (2017) Structure of the polycystic kidney disease TRP channel Polycystin-2 (PC2). *Nat. Struct. Mol. Biol.* **24**, 114–122
20. Oelstrom, K., and Chanda, B. (2016) Congruent pattern of accessibility identifies minimal pore gate in a non-symmetric voltage-gated sodium channel. *Nat. Commun.* **7**, 11608
21. Oelstrom, K., Goldschen-Ohm, M. P., Holmgren, M., and Chanda, B. (2014) Evolutionarily conserved intracellular gate of voltage-dependent sodium channels. *Nat. Commun.* **5**, 3420
22. Del Camino, D., and Yellen, G. (2001) Tight steric closure at the intracellular activation gate of a voltage-gated K(+) channel. *Neuron* **32**, 649–656
23. Kitaguchi, T., Sukhareva, M., and Swartz, K. J. (2004) Stabilizing the closed S6 gate in the Shaker Kv channel through modification of a hydrophobic seal. *J. Gen. Physiol.* **124**, 319–332
24. Sukhareva, M., Hackos, D. H., and Swartz, K. J. (2003) Constitutive activation of the Shaker Kv channel. *J. Gen. Physiol.* **122**, 541–556
25. Aryal, P., Sansom, M. S., and Tucker, S. J. (2015) Hydrophobic gating in ion channels. *J. Mol. Biol.* **427**, 121–130
26. Wang, W., Black, S. S., Edwards, M. D., Miller, S., Morrison, E. L., Bartlett, W., Dong, C., Naismith, J. H., and Booth, I. R. (2008) The structure of an open form of an *E. coli* mechanosensitive channel at 3. 45 A resolution. *Science* **321**, 1179–1183
27. Bass, R. B., Strop, P., Barclay, M., and Rees, D. C. (2002) Crystal structure of *Escherichia coli* MscS, a voltage-modulated and mechano-sensitive channel. *Science* **298**, 1582–1587
28. Jeon, J. P., Roh, S. E., Wie, J., Kim, J., Kim, H., Lee, K. P., Yang, D., Jeon, J. H., Cho, N. H., Kim, I. G., Kang, D. E., Kim, H. J., and So, I. (2013) Activation of TRPC4β by Gαi subunit increases Ca2+ selectivity and controls neurite morphogenesis in cultured hippocampal neuron. *Cell Calcium* **54**, 307–319
29. Yeh, B. I., Kim, Y. K., Jabbar, W., and Huang, C. L. (2005) Conformational changes of pore helix coupled to gating of TRPV5 by protons. *EMBO J.* **24**, 3224–3234
30. Chen, J., Kim, D., Bianchi, B. R., Cavanaugh, E. J., Faltynek, C. R., Kym, P. R., and Reilly, R. M. (2009) Pore dilation occurs in TRPA1 but not in TRPM8 channels. *Mol. Pain* **5**, 3
31. Chung, M. K., Güler, A. D., and Caterina, M. J. (2008) TRPV1 shows dynamic ionic selectivity during agonist stimulation. *Nat. Neurosci.* **11**, 555–564
32. Aryal, P., Abd-Wahab, F., Bucci, G., Sansom, M. S., and Tucker, S. J. (2014) A hydrophobic barrier deep within the inner pore of the TWIK-1 K2P potassium channel. *Nat. Commun.* **5**, 4377
33. Beck, A., Speicher, T., Stoerger, C., Sell, T., Dettmer, V., Jusoh, S. A., Abdulmughni, A., Cavalié, A., Philipp, S. E., Zhu, M. X., Helms, V., Wissenbach, U., and Flockerzi, V. (2013) Conserved gating elements in TRPC4 and TRPC5 channels. *J. Biol. Chem.* **288**, 19471–19483
34. Fecher-Trost, C., Wissenbach, U., Beck, A., Schalkowsky, P., Stoerger, C., Doerr, J., Dembek, A., Simon-Thomas, M., Weber, A., Wollenberg, P., Ruppert, T., Middendorff, R., Maurer, H. H., and Flockerzi, V. (2013) The in vivo TRPV6 protein starts at a non-AUG triplet, decoded as methionine, upstream of canonical initiation at AUG. *J. Biol. Chem.* **288**, 16629–16644
35. Zheng, W., Hussein, S., Yang, J., Huang, J., Zhang, F., Hernandez-Anzaldo, S., Fernandez-Patron, C., Cao, Y., Zeng, H., Tang, J., and Chen, X. Z. (2015) A novel PKD2L1 C-terminal domain critical for trimerization and channel function. *Sci. Rep.* **5**, 9460
36. Fernández, J. A., Skryma, R., Bidaux, G., Magleby, K. L., Scholfield, C. N., McGeown, J. G., Prevarskaya, N., and Zholos, A. V. (2011) Voltage- and cold-dependent gating of single TRPM8 ion channels. *J. Gen. Physiol.* **137**, 173–195
37. Courjaret, R., Hubrack, S., Daalis, A., Dib, M., and Machaca, K. (2013) The Xenopus TRPV6 homolog encodes a Mg^{+}-permeant channel that is inhibited by interaction with TRPC1. *J. Cell. Physiol.* **228**, 2386–2398
38. Yang, J., Wang, Q., Zheng, W., Tuli, J., Li, Q., Wu, Y., Hussein, S., Dai, X. Q., Shafiei, S., Li, X. G., Shen, P. Y., Tu, J. C., and Chen, X. Z. (2012) Receptor for activated C kinase 1 (RACK1) inhibits function of transient receptor potential (TRP)-type channel Pkd2L1 through physical interaction. *J. Biol. Chem.* **287**, 6551–6561
39. Peng, J. B., Chen, X. Z., Berger, U. V., Vassilev, P. M., Tsukaguchi, H., Brown, E. M., and Hediger, M. A. (1999) Molecular cloning and characterization of a channel-like transporter mediating intestinal calcium absorption. *J. Biol. Chem.* **274**, 22739–22746
40. Hoenderop, J. G., Nilius, B., and Bindels, R. J. (2005) Calcium absorption across epithelia. *Physiol. Rev.* **85**, 373–422
41. Peng, J. B. (2011) TRPV5 and TRPV6 in transcellular Ca^{2+} transport: regulation, gene duplication, and polymorphisms in African populations. *Adv. Exp. Med. Biol.* **704**, 239–275
42. Loukin, S., Su, Z., and Kung, C. (2011) Increased basal activity is a key determinant in the severity of human skeletal dysplasia caused by TRPV4 mutations. *PLoS One* **6**, e19533
43. Teng, J., Loukin, S. H., Anishkin, A., and Kung, C. (2015) L596–W733 bond between the start of the S4-S5 linker and the TRP box stabilizes the closed state of TRPV4 channel. *Proc. Natl. Acad. Sci. USA* **112**, 3386–3391
44. Freichel, M., Tsvilovskyy, V., and Camacho-Londoño, J. E. (2014) TRPC4- and TRPC4-containing channels. *Handb. Exp. Pharmacol.* **222**, 85–128
45. Akbulut, Y., Gaunt, H. J., Muraki, K., Ludlow, M. J., Amer, M. S., Bruns, A., Vasudev, N. S., Radtke, L., Willot, M., Hahn, S., Seitz, T., Ziegler, S., Christmann, M., Beech, D. J., and Waldmann, H. (2015) (−)−Englerin A is a potent and selective activator of TRPC4 and TRPC5 calcium channels. *Angew. Chem. Int. Ed. Engl.* **54**, 3787–3791
46. Bharate, S. S., and Bharate, S. B. (2012) Modulation of thermoreceptor TRPM8 by cooling compounds. *ACS Chem. Neurosci.* **3**, 248–267
47. Voets, T., Droogmans, G., Wissenbach, U., Janssens, A., Flockerzi, V., and Nilius, B. (2004) The principle of temperature-dependent gating in cold- and heat-sensitive TRP channels. *Nature* **430**, 748–754
48. Ma, S., G, G., Ak, V. E., Jf, D., and H, H. (2008) Menthol derivative WS-12 selectively activates transient receptor potential melastatin-8 (TRPM8) ion channels. *Pak. J. Pharm. Sci.* **21**, 370–378
49. Brelidze, T. I., Niu, X., and Magleby, K. L. (2003) A ring of eight conserved negatively charged amino acids doubles the conductance of BK channels and prevents inward rectification. *Proc. Natl. Acad. Sci. USA* **100**, 9017–9022
50. Salazar, H., Jara-Oseguera, A., Hernández-García, E., Llorente, I., Arias-Olguín, I. I., Soriano-García, M., Islas, L. D., and Rosenbaum, T. (2009) Structural determinants of gating in the TRPV1 channel. *Nat. Struct. Mol. Biol.* **16**, 704–710

Received for publication June 26, 2017.
Accepted for publication September 11, 2017.